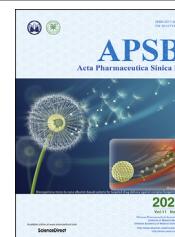




Chinese Pharmaceutical Association
Institute of Materia Medica, Chinese Academy of Medical Sciences

Acta Pharmaceutica Sinica B

www.elsevier.com/locate/apsb
www.sciencedirect.com



ORIGINAL ARTICLE

Cytosolic delivery of the immunological adjuvant Poly I:C and cytotoxic drug crystals *via* a carrier-free strategy significantly amplifies immune response



Xiaoqing Du^a, Yuqi Hou^a, Jia Huang^a, Yan Pang^a, Chenlu Ruan^a,
Wei Wu^b, Chenjie Xu^c, Hongwei Zhang^d, Lifang Yin^a, Wei He^{a,*}

^aDepartment of Pharmaceutics, School of Pharmacy, China Pharmaceutical University, Nanjing 211198, China

^bKey Laboratory of Smart Drug Delivery of Ministry of Education of China, School of Pharmacy, Fudan University, Shanghai 201203, China

^cDepartment of Biomedical Engineering, City University of Hong Kong, Kowloon, Hong Kong SAR, China

^dDepartment of Pharmaceutical Sciences, School of Pharmacy–Boston, MCPHS University, Boston, MA 02115, USA

Received 6 November 2020; received in revised form 15 January 2021; accepted 29 January 2021

KEY WORDS

Asynchronous release;
Co-delivery;
Immunogenicity;
Cancer cells;
Immunostimulant;
Paclitaxel;
Chemoimmunotherapy

Abstract Co-delivery of chemotherapeutics and immunostimulant or chemoimmunotherapy is an emerging strategy in cancer therapy. The precise control of the targeting and release of agents is critical in this methodology. This article proposes the asynchronous release of the chemotherapeutic agents and immunostimulants to realize the synergistic effect between chemotherapy and immunotherapy. To obtain a proof-of-concept, a co-delivery system was prepared *via* a drug-delivering-drug (DDD) strategy for cytosolic co-delivery of Poly I:C, a synthetic dsRNA analog to activate RIG-I signaling, and PTX, a commonly used chemotherapeutics, in which pure PTX nanorods were sequentially coated with Poly I:C and mannuronic acid *via* stimulating the RIG-I signaling axis. The co-delivery system with a diameter of 200 nm enables profound immunogenicity of cancer cells, exhibiting increased secretion of cytokines and chemokines, pronounced immune response *in vivo*, and significant inhibition of tumor growth. Also, we found that intracellularly sustained release of cytotoxic agents could elicit the immunogenicity of cancer cells. Overall, the intracellular asynchronous release of chemotherapeutics and immunomodulators is a promising strategy to promote the immunogenicity of cancer cells and augment the antitumor immune response.

*Corresponding author.

E-mail address: weihe@cpu.edu.cn (Wei He).

Peer review under responsibility of Chinese Pharmaceutical Association and Institute of Materia Medica, Chinese Academy of Medical Sciences.

<https://doi.org/10.1016/j.apsb.2021.03.014>

2211-3835 © 2021 Chinese Pharmaceutical Association and Institute of Materia Medica, Chinese Academy of Medical Sciences. Production and hosting by Elsevier B.V. This is an open access article under the CC BY-NC-ND license (<http://creativecommons.org/licenses/by-nc-nd/4.0/>).

© 2021 Chinese Pharmaceutical Association and Institute of Materia Medica, Chinese Academy of Medical Sciences. Production and hosting by Elsevier B.V. This is an open access article under the CC BY-NC-ND license (<http://creativecommons.org/licenses/by-nc-nd/4.0/>).

1. Introduction

Chemoimmunotherapy refers the combination of chemotherapy and immunotherapy^{1,2}. Chemotherapy uses drugs to kill or slow the growth of cancer cells while immunotherapy stimulates or restores the ability of the immune system to fight against cancer. In 2019, US Food and Drug Administration (FDA) approved the first chemoimmunotherapy regimen (Treanda-Rituxan-Polivy, an antibody–drug conjugate), for patients with relapsed or refractory diffuse large B-cell lymphoma. One of the keys in developing chemoimmunotherapy formulations is to circumvent the negative immunologic profile of chemotherapy and maximize the synergy of chemotherapy and immunotherapy. Delivery technology or platform has an unneglectable role for this job³. They can integrate chemotherapeutic and immunotherapeutic agents into one single system while improving the biodistribution, tissue penetration, half-life, and providing spatially and temporally controlled release^{4–6}. However, we noticed that the current drug delivery systems (DDSs) are mainly based on polymers or other materials, which unavoidably decreases the dosage of the drugs the system can deliver. For most traditional DDSs, their drug-loading capacity is lower than 10% (w/w)⁷. The low payload becomes more restricted for co-delivery since two or more than two drugs are required to be loaded. Furthermore, the conventional co-delivery systems are internalized *via* endo-lysosomes followed by dissociation, and simultaneously release their cargos to the cytoplasm within a limited period^{8–10}, frequently resulting in suboptimal therapeutic efficacy.

Previously, we have developed a co-delivery platform, namely drug-delivering-drug (DDD) strategy, which rod-like nanocrystals of an insoluble drug were utilized as a carrier to deliver a second biological drug or a small-molecular active compound^{11–15}. The drug-loading capacity of DDD can be as high as 60%–80% (w/w). Second, the DDD platform can enter cells without detainment by the endo-lysosomes and, as a result, significantly promote intracellular delivery of biopharmaceuticals^{11–15}. Additionally, the DDD platform allowed for sustained drug release from the drug nanocrystals and rapid release of the loaded biopharmaceutical after uptake^{11,12,15}.

Here, we hypothesized that this platform can be extended to the chemoimmunotherapy for the asynchronous release of chemotherapeutic agent and immunostimulant with high drug loading. This will eventually maximize the effect of chemoimmunotherapy. As a proof-of-concept, we co-delivered paclitaxel (PTX) and polyriboinosinic:polyribocytidylic acid (Poly I:C) to cancer cells using the DDD platform. PTX is a chemotherapeutic drug, triggering apoptosis of cancer cells^{16,17}. Whereas Poly I:C, a safe synthetic analog of double-stranded RAN (dsRNA) having little toxicity to the body¹⁸, is potent to activate the cytosolic retinoic acid inducible gene I (*RIG-I*), resulting in increased expression of IFN, chemokines and inflammatory cytokines and innate immune reactions^{19–22}. The co-delivery system was prepared by loading Poly I:C onto the pure rod-shaped PTX

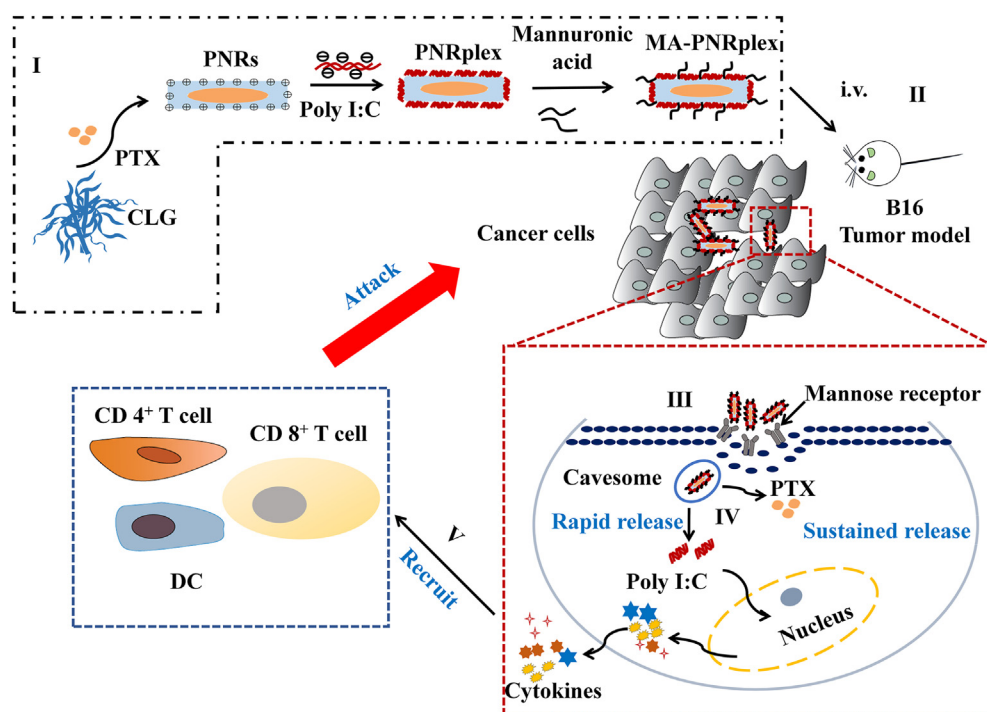
nanocrystals, named PTX nanorods (PNRs), which the PNRs were fabricated by using a simple antisolvent-precipitation method and cationic β -LG (CLG) as a stabilizer. To target cancer cells, a D-mannuronic acid (MA) was utilized to coat the PNR/Poly I:C complex (PNRplex) for mannose-receptor (MR) targeting (Scheme 1). We found that *via* enhancing the activation of the RIG-I signaling axis in cancer cells rather than immune cells, the developed co-delivery system markedly elicited the immunogenicity of cancer cells *via* promoted production of cytokines and chemokines and enabled profound enhancement in maturation of dendritic cells (DCs) and infiltration of CD4⁺ T cells and CD8⁺ T cells in the tumor.

2. Materials and methods

2.1. Materials and cells

Paclitaxel (PTX) was provided by Jiangsu Taxus Biochem Co., Ltd. (Jiangsu, China). β -Lactoglobulin (β -LG, No. L3908, 90% purity), polyinosinic:polycytidylic acid (Poly I:C, 99% purity), Cy5-Poly I:C, 3-(4,5-dimethylthiazol-2-yl)-2,5-diphenyltetrazolium bromide (MTT, 98% purity) and fluorescein isothiocyanate isomer I (FITC, 98% purity) were commercially purchased from Sigma–Aldrich (St. Louis, MO, USA). DiR was purchased from Biotium, Inc. (Hayward, CA, USA). D-Mannuronic acid sodium salt (MA, 99% purity) was purchased from Qingdaobozhihui Biochem Co., Ltd. (Qingdao, China). Nystatin was acquired from Aladdin Co., Ltd. (Shanghai, China). Primary antibody for RIG-I (ab45428), IRF3 (ab68481) and Phospho-IRF3, β -actin (ab37168), HRP-conjugated secondary antibody (ab205718), lysis buffer and protease inhibitor were purchased from Fcmacs Biotech Co., Ltd. (Nanjing, China). Annexin V-FITC/PI, DAPI, blocking buffer, Hematoxylin & Eosin Staining (H & E staining) Kits and TUNEL Kit were obtained from the Beyotime Institute of Biotechnology (Haimen, China). SDS-PAGE gel, ECL chemiluminescence Kit, BCA protein assay Kit, and mouse interferon- β (INF- β) ELISA Kits were from Guangzhou Jet Bio-Filtration Co., Ltd. (Guangzhou, China). The cell lines, fetal bovine serum (FBS), Dulbecco's modified Eagle's medium (DMEM), RPMI-1640, trypsin, 100 μ g/mL streptomycin and 100 IU/mL penicillin were obtained from Nanjing Key GEN Biotech Co., Ltd. (Nanjing, China). Anti-mouse monoclonal antibodies labeled with fluorochromes (CD11c, CD86, CD3e, CD4, CD8a) were supplied by Biolegend (San Diego, USA). Mouse C-X-C motif chemokine 10 (CXCL-10) ELISA Kits, mouse C-C motif chemokine ligand 5 (CCL-5) ELISA Kits and mouse interleukin-6 (IL-6) ELISA Kits were from Multiscience (Lianke) Biotech, Co., Ltd. Tumor lymphocyte separation solution Kit and spleen lymphocyte separation Kit were purchased from Tianjin Haoyang Biological Manufacture Co., Ltd. (Tianjin, China).

Female C57BL/6 mice aged 6–8 weeks were provided by Qinglongshan Animal Center (Nanjing, China). The animals acquired care that followed the Principles of Laboratory Animal Care



Scheme 1 Illustration of the targeted co-delivery of the immunological adjuvant Poly I:C and cytotoxic drug nanorods for immunotherapy by using a strategy of drug-delivering-drug (DDD). (I) Preparation of MA-PNRplex by loading Poly I:C on paclitaxel (PTX) nanorods (PNRs), followed by MA coating. Purposed mechanism: (II) after intravenous injection, (III) MA-PNRplex is internalized *via* caveosomes, a pathway bypassing endo-lysosomes, (IV) continue releasing of PTX while rapidly release Poly I:C, (V) Poly I:C promotes the secretion of chemokines and cytokines through RIG-I pathway and recruits immune cells to poison the cancer cells; and subsequently, the cumulative release of PTX generates additional toxicity to the cancer cells, eventually achieving chemoimmunotherapy.

and the Guide for the Care and Use of Laboratory Animals. All animal experiments were approved by the Institutional Animal Care and Ethics Committee of China Pharmaceutical University, China.

2.2. Preparation and characterization

PTX nanorods (PNRs) were prepared by using a simple antisolvent-precipitation method, with cationic β -LG (CLG) as a stabilizer as described in previous reports^{23,24}. Briefly, 10 mL CLG solution (1 mg/mL) was mixed with organic phase, 0.5 mL PTX solution (40 mg/mL in dimethyl sulfoxide) under stirring conditions and treated with an ultrasonic probe (20–25 kHz, Scientz Biotechnology Co., Ltd., Ningbo, China) at 250 W for 10 min. The entire preparation was performed at 4 °C.

PNR/Poly I:C complex (PNRplex) and MA-coated PNRplex (MA-PNRplex) were prepared by the electrostatic attraction method. In brief, PNRplex was prepared through mixing PNRs and an equal volume solution of Poly I:C (100 μ g/mL) followed by incubation at room temperature for 30 min. MA-PNRplex was fabricated by adding MA solution to a dispersion of PNRplex under vigorous stirring. The MA concentration of coating was optimized regarding the diameter and surface charge of the nanoparticles. Dye-labeled nanoparticles were prepared using a similar procedure. FITC-labeled nanoparticles were prepared by dissolving the dye with PTX in dimethyl sulfoxide together as the organic phase prior to mixing with the CLG solution. Dual-labeled PNRplex or MA-PNRplex were fabricated by assembling Cy5-Poly I:C on FITC-nanoparticles.

The nanoparticles were characterized in terms of the average particle size, polydispersity index (PDI) and zeta potential using a

90 Plus Particle Size Analyzer (Brookhaven Instruments, Holtsville, NY, USA). A transmission electron microscopy (TEM, JEM-1230 TEM, Tokyo, Japan) was used to examine the morphology of nanoparticles. One drop of the prepared nanoparticles was placed to a copper mesh, followed by drying at 25 °C, staining with 2% (w/w) phosphotungstic acid for 1 min, removing the excess phosphotungstic acid, and air-drying.

The encapsulation efficiency (EE) and drug loading (DL) of PTX and Poly I:C were measured by Eqs. (1)–(4):

$$\text{EE (\% of PTX)} = \left(\frac{\text{Amount of PTX in MA-PNRplex}}{\text{Amount of PTX added}} \right) \times 100 \quad (1)$$

$$\text{DL (\% of PTX)} = \left(\frac{\text{Amount of PTX in MA-PNRplex}}{\text{Amount of MA-PNRplex free-dried powder}} \right) \times 100 \quad (2)$$

$$\text{EE (\% of Poly I:C)} = \left(\frac{\text{Amount of Poly I:C}}{\text{Amount of Poly I:C added}} \right) \times 100 \quad (3)$$

$$\text{DL (\% of Poly I:C)} = \left(\frac{\text{Amount of Poly I:C}}{\text{Amount of free-dried MA-PNRplex}} \right) \times 100 \quad (4)$$

The content of PTX was determined by a high-performance liquid chromatography (HPLC) system (SHIMAZU LC-10AT, Kyoto, Japan) under the conditions described in a previous report²⁵. The concentration of Poly I:C was examined by indirectly measuring the absorbance of free Poly I:C in the supernatant collected upon ultracentrifugation at 260 nm using a Nano-100 (Thermo Fisher Scientific).

Agarose gel electrophoresis was conducted to confirm the loading of Poly I:C in the nanoparticles. Briefly, PNRplex with various mass ratios of CLG/Poly I:C and positive control (naked Poly I:C) were cultured with $5 \times$ loading buffer containing GelRed (Generay Biotechnology, China) for 30 min, loaded into the respective wells of the gel at 80 V for 30 min, and finally was analyzed using a Bio-Rad high-sensitivity chemiluminescence imaging system (Chemidoc XRS+, USA). The serum stability of MA-PNRplex was performed by incubation in 10% fetal bovine serum (FBS) solution at 37 °C and was subjected to turbidity determination at specific time intervals using UV-Vis spectroscopy (UV-2450, Shimadzu, Japan).

The release of PTX from the nanoparticles was evaluated by the dialysis method on a shaker with a shaking speed of 100 rpm at 37 °C. In brief, 3.5 kDa dialysis bag were loaded with 1 mL of the samples with a PTX concentration of 0.2 mg/mL and was then immersed in 30 mL of release medium containing 0.2% Tween 80 at pH 7.4 or pH 5.0. At the predetermined time points, 1 mL of dialysis solution was sampled, along with a supply of 1 mL of fresh medium. The content of PTX in the samples was determined using an HPLC system as described in a previous report²⁵.

2.3. Cellular uptake

To determine the expression of mannose receptors on murine melanoma B16F10 cells, the cells were cultured in a confocal dish at a density of 1×10^5 cells/well, suspended in complete DMEM overnight, incubated with DiI at a concentration of 1 mmol/L at 37 °C for 1 h, fixed by 4% paraformaldehyde for 10 min at 37 °C, blocked by 5% BSA at 37 °C for 1 h, stained with Alexa Fluor® 488-labeled anti-mannose receptor at 4 °C overnight, and washed with PBS, stained with DAPI, and finally observed with confocal laser scanning microscope (CLSM, Carl Zeiss, Germany).

For cellular uptake studies, the cells (1×10^5) were cultured with dual-labeled nanoparticles with a FITC concentration of 10 µg/mL or a Cy5 concentration of 2 nmol/L in a serum-free culture medium at 37 °C. At predetermined time points, the cells were harvested for flow cytometry analysis (Cytomics™ FC 500, Beckman Coulter) and observation by CLSM.

To investigate the role of mannose receptors in the cellular uptake of MA-PNRplex, cells were preincubated with 1 mg/mL MA for 1 h, followed by being cultured with FITC-labeled nanoparticles at a FITC concentration of 10 µg/mL at 37 °C for 4 h. To explore the endocytic pathway, the cells were treated by endocytic inhibitors, nystatin (10 mmol/L), for 30 min at 37 °C in advance and then, were incubated with dual-labeled MA-PNRplex.

2.4. In vitro cytotoxicity and apoptosis assay

Cell viability was detected by MTT assay. In brief, cells were seeded in 96-well plates (5000 cells/well) and incubated for 24 h at 37 °C before the administration of drugs. The cells were treated with different formulations at various concentrations for 48 h and incubated with 20 µL of MTT (5 mg/mL) for 4 h and 200 µL of dimethyl sulfoxide, respectively. The absorbance of each well was measured by a microplate reader (Thermo, Varian Flash).

Cell apoptosis was evaluated by Annexin V-FITC/PI double staining assay. In brief, B16F10 cells were seeded in a 6-well plate at a density of 2×10^5 cells per well, treated with different nanoparticles at a fixed PTX concentration of 10 µg/mL or Poly I:C at 2.5 µg/mL for 48 h at 37 °C, and stained with FITC-conjugated Annexin V (5 µL) and PI (5 µL) according to the protocol for analysis by flow cytometry.

2.5. Western blot (WB) assay and ELISA assay in vitro

B16F10 cells in 6-well plates at a density of 2×10^5 cells/well were incubated with various nanoparticles at a fixed PTX concentration of 10 µg/mL or Poly I:C concentration of 2.5 µg/mL for 12 h at 37 °C in advance, and were cultured in free-serum media for another 48 h.

For WB analysis, the treated cells were collected, lysed in cold lysis buffer for 30 min and centrifuged at $10,000 \times g$ for 10 min at 4 °C, followed by protein determination with a BCA protein assay Kit, mixing with loading buffer and boiled at 90 °C for 5 min, protein separation by SDS-PAGE, transferring onto PVDF membranes, blocking with 5% skim milk for 1 h at room temperature, treatment with anti-RIG-I, anti-IRF3 and anti-P-IRF3 overnight at 4 °C, incubation with HRP-linked secondary antibody for 1 h, and being dyed with ECL chemiluminescence Kit. The images were taken from a G: Box ChemiXR5 (Syngene, Cambridge, UK) using β -actin as the internal reference. The quantification of the bands was analyzed by an ImageJ software (National Institutes of Health) with β -actin for normalization.

For the ELISA assay, supernatants of treated cells were collected and centrifuged at 5000 rpm for 15 min. The expression levels of IFN- β , CXCL-10, CCL5, and IL-6 in the supernatant were determined by ELISA Kit according to the protocol.

2.6. Co-culture study in vitro

The co-culture study and CFDA-SE-labeled B16F10 cells were performed as described previously^{26,27}. The supernatants were collected after incubation of B16F10 cells with various nanoparticles at a fixed PTX concentration of 10 µg/mL or Poly I:C concentration of 2.5 µg/mL for 48 h at 37 °C. ELISA assay was utilized to confirm the concentration of the chemokines and cytokines in the supernatants. Splenocytes were isolated from C57BL/6 mice and adjusted a density of 4×10^6 cells/mL. Whereas CFDA-SE labeled B16F10 cells were resuspended to a density of 1×10^5 cells/mL in DMEM medium. Then CFDA-SE labeled B16F10 cells (0.5 mL) were cultured with equal volume of splenocytes for 4 h in a 12-well plate and were treated with the collected supernatants for another 24 h. Finally, the B16F10 cells and splenocytes were harvested and stained with propidium iodide (PI). The death rate of B16F10 cells (CFDA-SE⁺/PI⁺) was assayed by flow cytometry after gating on the CFDA-SE-labeled B16F10 cells. CFDA-SE labeled B16F10 cells without being cultured with splenocytes and supernatants were used as control.

2.7. In vivo biodistribution and tumor targeting

B16F10 tumor-bearing C57BL/6 mice were used in biodistribution studies and anti-tumor activities. B16F10 cells (1×10^7 cells/mL) were subcutaneously injected into the

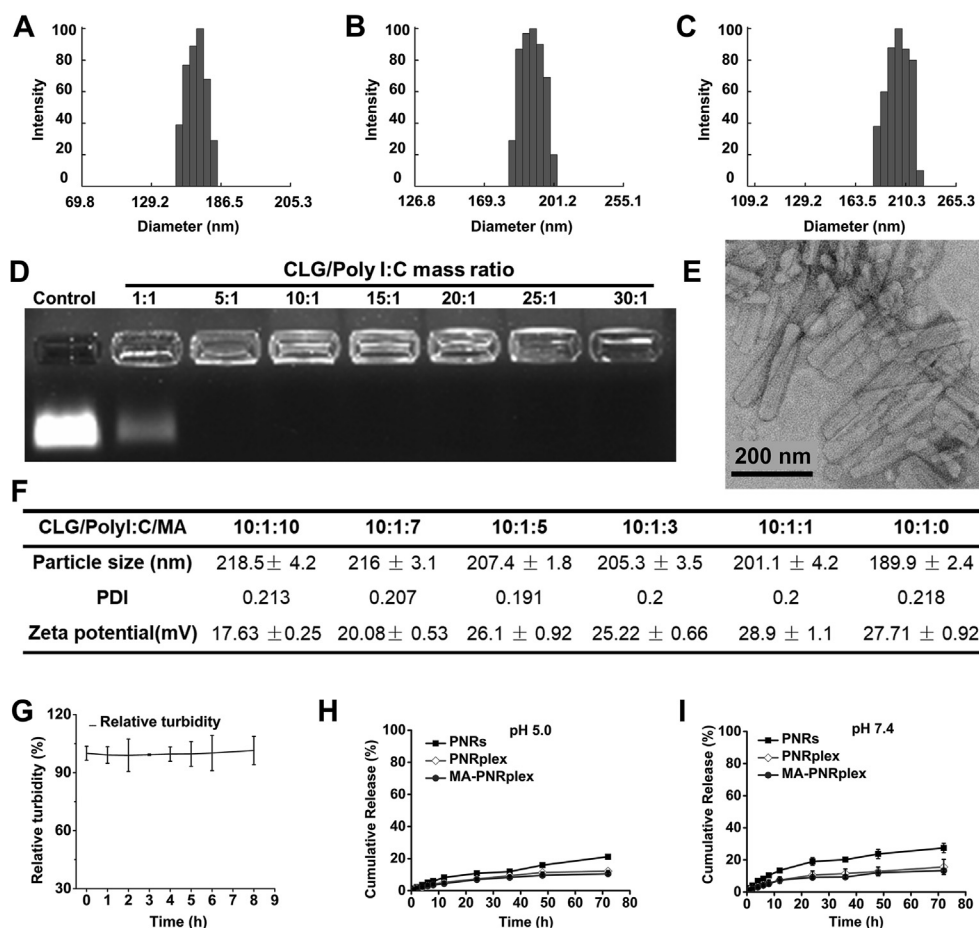


Figure 1 Characterization of the nano-complex. Size distribution of PNRs (A), PNRplex (B), and MA-PNRplex (C). (D) Gel electrophoresis of PNRplex with different mass ratios of stabilizer (CLG)/Poly I:C ranging from 1 to 30. (E) TEM observation of MA-PNRplex from the optimized formulation. (F) Particle size, PDI and zeta potential of MA-PNRplex with different mass ratios of CLG/Poly I:C/MA. (G) Serum stability of MA-PNRplex in 10% FBS studied by determination of turbidity by UV-spectroscopy at 260 nm at 37 °C within an 8-h period (mean ± SEM, $n = 3$). (H and I) *In vitro* release profile of PTX from PNRs, PNRplex and MA-PNRplex at 37 °C for 72 h (H, pH 7.4; I, pH 5.0).

axilla region of the mice. When the tumor volume reached about 50 mm³, the mice were selected for the subsequent experiments.

The mice were injected 200 μL of DiR-labeled nanoparticles *via* the tail vein at a fixed dose of 0.5 mg/kg of DiR based on the animal's body weight. At specific time points after dosing, the anesthetized mice were imaged *in vivo* to detect fluorescence intensity using an imaging system (IVIS Spectrum, PerkinElmer, USA) at an excitation wavelength of 748 nm and an emission wavelength of 780 nm. At the end of the experiment, the mice were sacrificed to harvest the major organs and tumors to detect the *ex vivo* fluorescence intensity.

2.8. *In vivo* therapeutic effects

The B16F10 tumor-bearing C57BL/6 mice were randomly divided into eight groups (6 mice per group) and were dosed with 0.2 mL of different nanoparticles every 3 days for 5 times *via* the tail vein at a fixed PTX dose of 10 mg/kg and Poly I:C dose of 0.5 mg/kg or 1 mg/kg body weight. The body weight and tumor volume were recorded every 2 days during the treatment. On Day 13, all mice were sacrificed to harvest the tumors and major tissues for subsequent experiments. The extracted tumors were frozen and

sectioned for hematoxylin-eosin (H&E) staining, TUNEL assay and Ki67 staining.

2.9. Immune response *in vivo*

Single-cell suspensions from the extracted spleens and tumors were obtained according to the protocol from Tumor and Spleen Lymphocyte Separation Kit. In brief, the resected tumors and spleens were weighed, mechanically cut into small pieces, and gently ground through a 70-μm cell strainer followed by centrifugation, resuspending, isolation of immune cells, and washing three times. Activated and mature CD86⁺ CD11c⁺ DCs were detected by flow cytometry. Whereas for the measurement of CD4⁺ T cells and CD8⁺ T cells, the cells were stained with anti-CD3e, anti-CD8 and anti-CD4 antibodies, according to the instruction of the Kit.

The sections of tumors and spleens were immersed in PBS and homogenized in cold PBS. Then the serum and supernatant of homogenates were centrifuged at 10,000×g for 10 min at 4 °C. The levels of cytokines and chemokines in the isolated tumors and spleens and serum were analyzed by ELISA Kit according to the protocol. The levels of RIG-I, IRF3 and P-IRF3 in the tumors were examined by WB analysis.

2.10. Statistical analysis

Data are represented as mean values \pm standard deviation (SD). The inter-group differences were evaluated by one-way ANOVA with *post hoc* Tukey's test and $P < 0.05$ indicates significant differences.

3. Results

3.1. Preparation and characterization of nanoparticles

Paclitaxel nanorods (PNRs) were prepared through an antisolvent-precipitation method by using CLG as the stabilizer. Poly I:C and MA were then loaded onto the 175 nm PNRs (Fig. 1A) sequentially to prepare MA-PNRplex (Scheme 1). The formulation of PNRplex was optimized by altering the mass ratio of CLG/Poly I:C. The assay of agarose gel electrophoresis displayed that the bands of Poly I:C disappeared when the mass ratio was ≥ 5 and demonstrated Poly I:C was well loaded (Fig. 1D). The loading of Poly I:C could in general increase the diameter and decrease the positive charge of PNRplex (Supporting Information Figs. S1A and S1B). PNRplex with a mass ratio of 10 and a diameter of 190 nm (Fig. 1B) was selected for MA coating due to the high loading of Poly I:C and enhanced stability against disassociation *in vitro* among the formulations. The coating of MA increased the size and reduced the positive-charge of MA-PNRplex, along with the increase in MA concentrations (Fig. 1F, Figs. S1C and S1D). MA-PNRplex with CLG/Poly I:C/MA mass ratio of 10:1:10 and with a size of 218 nm (Fig. 1C) was selected for further study owing to the least positive surface charge. Determination by HPLC method demonstrated that the drug-loading in the optimized formulation of MA-PNRplex is approximately 64% (*w/w*) for PTX and 3% for Poly I:C, along with encapsulation efficacy of 99% and 83% for PTX and Poly I:C, respectively. TEM images displayed MA-PNRplex had a rod-like structure with an average length of 200 nm (Fig. 1E). The little alteration in turbidity, assayed by UV-Vis spectroscopy upon 9-h incubation in 10% FBS, implied the nanoparticles were stable against serum-mediated aggregation and dissociation after systemic administration (Fig. 1G).

The *in vitro* PTX release from the preparations was performed by a dialysis method in media at pH 5.0 and 7.4 (Fig. 1H and I). Approximately 30% of PTX was released from PNRs within 72 h in both conditions, whereas less than 15% of PTX was released from PNRplex and MA-PNRplex. The results demonstrated that these nanoparticles allowed for sustained release of the small-molecular cytotoxic agent, PTX, over time and the loading of Poly I:C was able to further slow the release.

3.2. Improved internalization in cancer cells mediated by MR-targeting

First, the expression of the mannose receptor (MR) on B16F10 cells was confirmed by using Alexa Fluor® 488-labeled anti-mannose receptor. As displayed in Supporting Information Fig. S2, yellow fluorescence locating on the cell surface demonstrated the colocalization of MR and cell membrane and indicated the high expression of MR.

In order to study the role of MR in cellular uptake, B16F10 cells were cultured with free MA in advance to block the receptors, and then incubated with FITC-MA-PNRplex. The

uptake of the nanoparticles was reduced by approximately 70% at the MA concentration of 100 $\mu\text{g/mL}$ compared with the control group which was not pretreated with MA (Supporting Information Fig. S3A), indicating that MR is of importance to mediate the uptake. Also, the internalization was time-dependent in a 4-h period (Figs. S3B and S3C). Interestingly, obvious pink spots in the cells were displayed at 4 h post-incubation, which implied that the dual-labeled nanoparticles were not broken after internalization (Fig. S3C). The presence of the unbroken nanoparticles in the cells was ascribed to the internalization *via* bypassing the endo-lysosomal system. As depicted in Fig. S3D, the pretreatment with the caveolar inhibitor, nystatin, decreased the uptake of the nanoparticles significantly ($P < 0.01$). Accordingly, the nanoparticles were internalized mainly *via* a caveolar pathway. It is well known that caveolar endocytosis is closely associated with the cytosolic delivery without entrapment within the endo-lysosomes^{15,28,29}. Herein, we demonstrated that the cellular uptake of the nanoparticles could be enhanced by MA coating and, moreover, was governed predominantly by a nonendo-lysosomal pathway.

Next, the cytotoxicity of various formulations to B16F10 cells was investigated. As expected, due to the improved cellular internalization, MA-PNRplex exhibited the strongest toxicity against the cancer cells at all measured concentrations among these nanoparticles (Supporting Information Fig. S4A). Moreover, the MA-PNRplex have a higher ability to induce apoptosis of the cancer cells compared with other groups, along with >5 -fold increase in apoptosis rate over PNRs without loading Poly I:C (Fig. S4B and C, $P < 0.001$).

3.3. Significant improvement of anti-tumor effect *in vivo*

The biodistribution and tumor accumulation in B16F10 tumor-bearing mice were studied *via* intravenous injection of free DiR or DiR-labeled nanoparticles. The nanoparticles largely accumulated in the two organs of the reticuloendothelial system, liver and spleen, at 24 h after injection (Fig. 2A, B and D). However, surprisingly, the accumulation of DiR-MA-PNRplex in the tumor is comparable with that in the two organs and demonstrated its potent tumor-targeting ability. Furthermore, the fluorescence intensity from DiR-MA-PNRplex was approximately 1.5-fold greater than that from DiR-PNRplex at all time points (Fig. 2C), which highlighted the significance of MA coating.

To examine the *in vivo* anti-tumor efficacy, the B16F10 tumor-bearing mice were dosed with various nanoparticles. Compared with the saline group on Day 13 post administration, the growth of tumor was inhibited by 6% for Poly I:C group, 15% for free Taxol/Poly I:C (combined use of free PTX and Poly I:C) group, 56% for PNR group, 68% for PNRplex group, 75% and 81% for MA-PNRplex (low) and (high) groups, respectively (Fig. 3A and B). MA-PNRplex inhibited tumor growth with the highest efficacy, amid the formulations. In particular, intracellular delivery of Poly I:C using PNRs reduced the tumor volume by approximately 11-fold for PNRplex, 13- and 14-fold for MA-PNRplex at low dose and high dose, respectively, compared with free Poly I:C. The weight examination of the extracted tumors confirmed the results of tumor growth inhibition (Fig. 3D). Little change in the animals' body weight indicated the nanoparticles had no toxicity to the body (Fig. 3C). To further test the anti-tumor activities, the extracted tumors were examined *in situ* for apoptosis and proliferation. Again, most profound necrosis, apoptosis and anti-proliferation were displayed in the groups treated with MA-

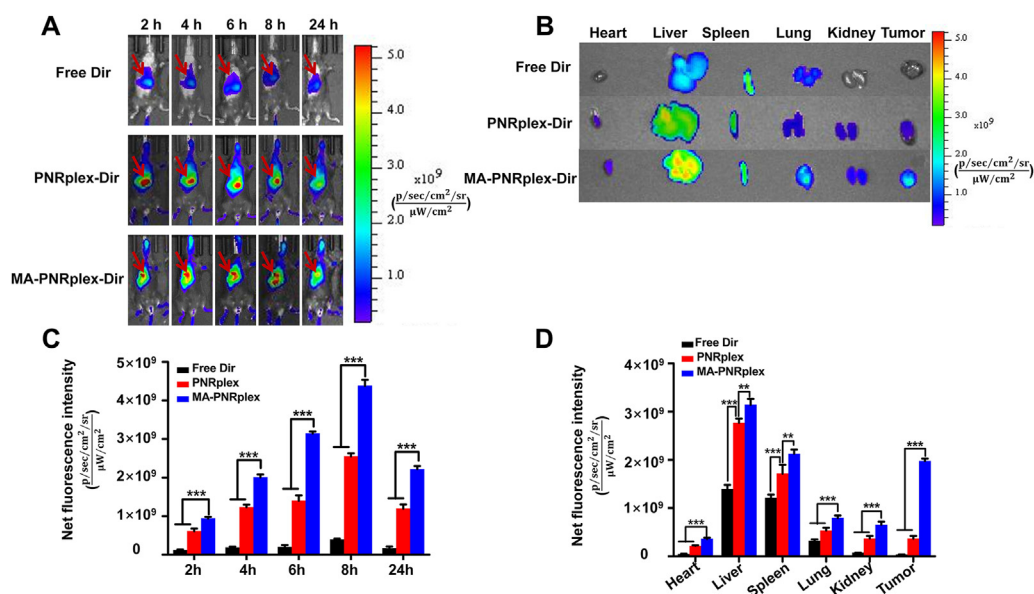


Figure 2 Biodistribution and tumor accumulation. (A) *In vivo* fluorescence imaging of the B16F10 tumor-bearing C57BL/6 mice after intravenous injection with free DiR, DiR-PNRplex and MA-DiR-PNRplex at different time points. (B) *Ex vivo* imaging of the excised tumors and the major tissues and fluorescence intensity of the DiR signal in the (C) isolated tumors and (D) the major tissues at 24 h after administration (mean \pm SEM, $n = 3$, $**P < 0.05$ and $***P < 0.001$).

PNRplex (low and high doses, Fig. 3E). MA-PNRplex (low and high doses) increased the apoptosis rate by > 2.5 -fold over the group treated with Poly I:C ($P < 0.001$, Fig. 3F), confirmed by the proliferation analysis (Fig. 3G). Taken together, MA-PNRplex efficiently accumulated in the tumors and markedly inhibited the tumor growth.

3.4. Pronounced immune response *in vivo* via activating DCs and recruiting T-helper cells and cytotoxic T cells

Poly I:C, a commonly used immunostimulatory adjuvant in cancer treatment³⁰, can enhance the immune response by triggering signaling pathways in immune cells, such as DCs, fibroblasts and phagocytic cells^{31–34}. Poly I:C is efficient to mature and activate DCs, enhance specific antigen cross-presentation to T-helper cells ($CD4^+$), cytotoxic T cells ($CD8^+$) or natural killer T cells and, therefore, elevate the activation of T cells against cancer cells^{35–37}. Herein, the *in vivo* immune response was investigated by assaying these immune cells in the collected tumors and spleens at the end of treatment. The maturation of DCs in the tumor was assayed *via* detection of markers of CD86 and CD11c. As shown in Fig. 4A and Supporting Information Fig. S5A, free Poly I:C or free Taxol/Poly I:C had little effects on the maturation of DCs in the tumor, whereas PNRplex, MA-PNRplex at low or high dose significantly improved the maturation and increased the DCs population for approximately 7-, 13- and 17-fold over the groups of free Poly I:C, respectively. In addition, the infiltration of $CD4^+$ T cells and $CD8^+$ T cells in the tumors was measured *via* determination of the markers of CD3e, CD4 and CD8. Markedly improved infiltration of $CD8^+$ (Fig. 4C and Fig. S5C) and $CD4^+$ T cells (Fig. 4B and Fig. S5B) in the tumors was displayed after dosing MA-PNRplex, unveiling the immune response of T cells. The spleens are a part of the body's lymphatic system and are essential to the innate and adaptive immune response³⁸, and the elicited maturation of DCs and accumulation of T cells in the

tumors is always proportional to that in the spleen. Therefore, the expanding population of the immune cells in the spleen was investigated as well. Similar enhancement in expanding population of the immune cells was observed in the spleens (Fig. 4D–F and Fig. S5D–S5F). In particular, MA-PNRplex significantly elevated the recruitment of the immune cells in the tumors and spleens than PNRplex ($P < 0.01$), demonstrating that the MA coating played a vital role to the immune augmentation. Overall, these results indicated that dosing MA-PNRplex enabled extremely stronger immunostimulatory potency.

3.5. Significantly increased secretion of cytokines and chemokines in the tumor microenvironment

Immune augmentation is always closely associated with the increased secretion of chemokines and cytokines. Tumor-derived IFN- β is critical to the activation of DCs and contributes to cross-present tumor-associated antigen to naïve $CD8^+$ T cells³⁹. IL-6 is also associated with the regulation of inflammatory reactions, DCs maturation and T cell immunity^{40,41}. CXCL-10 and CCL-5 are robust to recruit T cells, natural killer (NK) cells and DCs to the tumors⁴². In the study, we measured the release of these cytokines and chemokines with ELISA Kits in the collected tumors, spleens and serum at the end of treatment (Fig. 5 and Supporting Information Fig. S6). Administration of free Poly I:C, Taxol/Poly I:C, or PNRs increased IFN- β by < 0.6 fold compared with the control (saline), whereas injection of PNRplex or MA-PNRplex at low or high dose upregulated the level of cytokine by 1.8-, 2-, and 2.5-fold, respectively (Fig. 5A). Dosing the three complex of PNR/Poly I:C elevated the level of IL-6 by 1–2.5-fold in the tumors in comparison to the control (Fig. 5B). Furthermore, the treatment with the three complexes promoted the chemokines by 2–2.8-fold for CCL-5 and by 1.5–2.5-fold for CXCL-10 over the control, while dosing free Poly I:C, Taxol/Poly I:C, or PNRs had little influence on the production of the two chemokines (Fig. 5C and D).

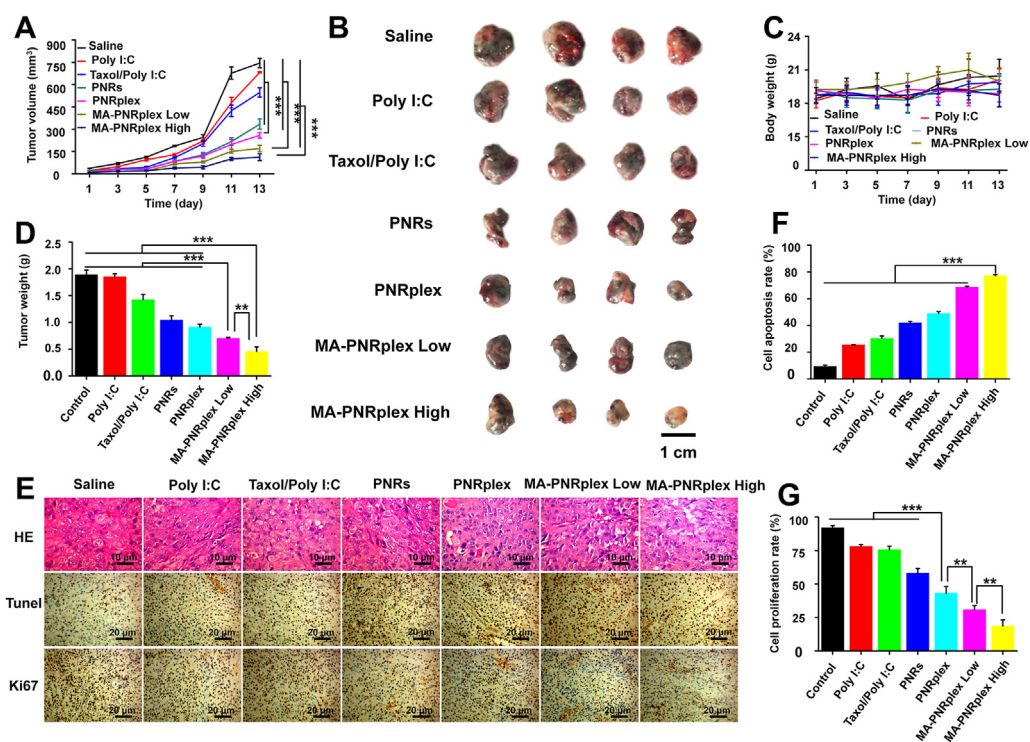


Figure 3 *In vivo* anti-tumor efficacy. Various formulations (0.2 mL) were administered to C57BL/6 tumor-bearing mice *via* tail vein injections every 3 days at a PTX dose of 10 mg/kg or a Poly I:C dose of 500 μ g/kg; whereas MA-PNRplex were injected at two doses, 10/0.5 mg/kg (low) and 10/1 mg/kg (high) for PTX/Poly I:C. Saline was used as a negative control. At the end of the treatment, tumor and major tissues were extracted for the further experiments. (A) Tumor volume growth curves ($n = 6$, $***P < 0.001$). (B) Representative tumors isolated from tumor-bearing mice collected at the end of treatment. (C) Body weight changes curves ($n = 6$, $***P < 0.001$). (D) Tumor weight ($n = 6$, $***P < 0.001$). (E) H&E staining, TUNEL and Ki67 examinations of tumors. For H&E examination, the nuclei were stained blue while the cytoplasm and extracellular matrix are stained red. The absence of nuclei represents the necrosis of tumor cells. The scale bar is 10 μ m. In the TUNEL and Ki67 assay, brown-stained cells represent positive cells. The scale bar is 20 μ m. Quantification assay of cell apoptosis (F) and cell proliferation (G) ($n = 3$, $**P < 0.01$ and $***P < 0.001$).

As depicted in Fig. 4D–F, the dosing of PNRplex, low and high dose of MA-PNRplex promoted the activation and proliferation of immune cells in the spleens. Accordingly, the levels of these cytokines and chemokines in the peripheral blood and spleens were assayed. Significantly increased levels of IFN- β (Fig. S6A), IL-6 (Fig. S6B), CCL-5 (Fig. S6C) and CXCL-10 (Fig. S6D) in the spleens were displayed post-administration of these complex. The elicited levels of the cytokines and chemokines were detected in the serum as well (Figs. S6E–H).

3.6. Cytokines and chemokines generated from cancer cells enhanced immune activity *in vitro*

Besides immune cells, other non-immune cells like endothelial cells and cancer cells are also able to secrete chemokines and cytokines under certain conditions⁴³. As demonstrated in Fig. S3A, MA-PNRplex targeted well to B16F10 cells and improved its uptake. Therefore, we hypothesized the increased chemokines and cytokines *in vivo* were mainly produced by the cancer cells. Here, the secretion of IFN- β , IL-6, CXCL-10 and CCL-5 from B16F10 cells was assayed after incubation with various formulations. Intracellular delivery of Poly I:C and PNRs by using the complex, PNRplex or MA-PNRplex, promoted the secretion of IFN- β over other groups (Fig. 6A).

Particularly, the level of IFN- β from the group treated with MA-PNRplex at low or high dose was higher than that from PNRplex ($P < 0.05$), indicating targeting the cancer cells enabled increased production of the cytokine. Similarly, elevated levels of IL-6, CCL-5 and CXCL-10 from the cancer cells were shown after incubation with MA-PNRplex at low and high dose (Fig. 6B–D). In addition, the increased production of the four factors from the cancer cells treated with various formulations was proportional to that *in vivo* (Fig. 5). Therefore, targeted co-delivery of Poly I:C and PNRs to the cancer cells are crucial to the increased production of the chemokines and cytokines.

In order to determine the effect of the secreted chemokines and cytokines on the activation of immune cells and immune cytotoxicity against cancer cells, a co-culture study was performed by incubating the supernatants collected from the cancer cells treated with various formulations with the splenocytes isolated from mice and CFDA-SE labeled B16F10 cells. The apoptosis rates from the groups treated with PNRplex or MA-PNRplex at low or high dose were of 14%, 18% and 25%, respectively, and are 4–7-fold increase over that from the formulation Taxol/Poly I:C (Supporting Information Figs. S7A and S7B). Interestingly, the drug nanorods, PNRs, also showed enhanced ability to activate the splenocytes and killed the cancer cells compared with free Poly I:C and Taxol/Poly I:C ($P < 0.01$). The results demonstrated that the secreted

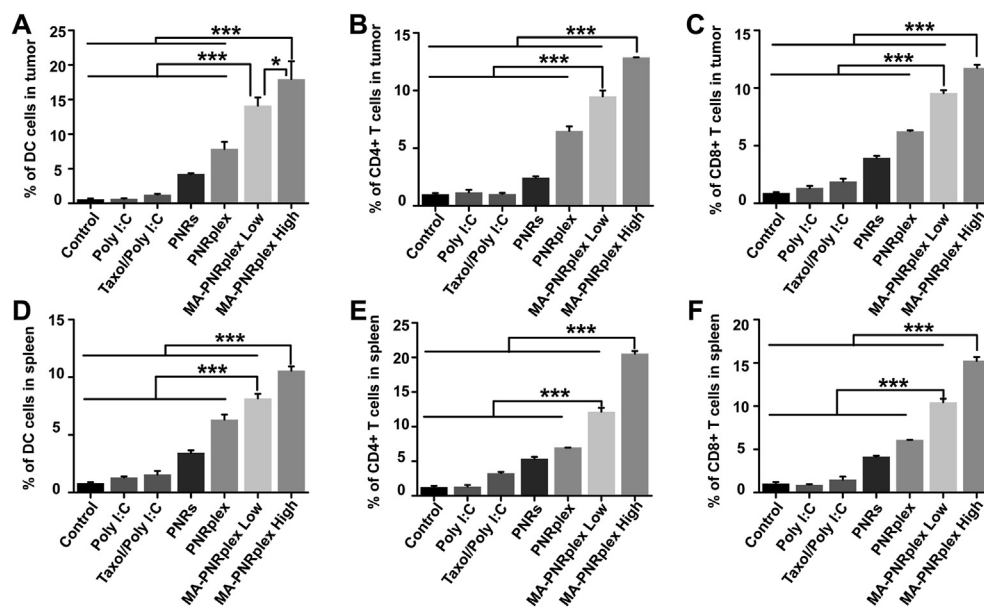


Figure 4 Immune response *in vivo*. Immune response analysis in the tumors and spleens sampled on Day 13 at the end of treatment. The percentage of DC cells and T cells within the tumor (A–C) and the spleen (D–F) (mean \pm SEM, $n = 3$, $*P < 0.05$, $***P < 0.01$). The immune cells were analyzed by collection of single cell suspensions from the tissues, staining with antibodies and determination with flow cytometry.

chemokines and cytokines from the cancer cells could stimulate the immune cells *in vitro* and improve their ability to induce apoptosis in cancer cells, whereas the secreted level plays an important role in the activation.

3.7. Enhanced immunostimulatory efficacy via activation of RIG-I-IRF3/P-IRF3 signaling axis in cancer cells

The production of chemokine and cytokine is always related to the stimulation of the signaling pathway. Poly I:C can interact with the TLRs within the endosomal compartment⁴⁴, RIG-I or RIG-I-like receptors in the cytoplasm⁴⁵. To be more specific, *via* recognition by RIG-I and involvement of IRF3/P-IRF3 signaling, Poly I:C is potent to increase the production of interferons (IFNs), chemokines and inflammatory cytokines and thus promote an immune response^{19–22}. Here, we detected the RIG-I-IRF3/P-IRF3 signaling axis by WB assay in B16F10 cells treated with various formulations. Compared with the control treated with PBS, the groups treated with drug-containing formulations upregulated RIG-I (Fig. 7A and B); however, for the P-IRF3/IRF3 ratio, highest expression level was displayed in the groups administered with MA-PNRplex at low or high dose, along with 5–6-fold increase in contrast with that from saline-treated group (Fig. 7A and C). Again, PNRs significantly elevated the level of P-IRF3/IRF3 ratio over Poly I:C or taxol/Poly I:C ($P < 0.01$), consistent with the results of cytokine- and chemokine-secretion *in vitro* (Fig. 6). In order to confirm the *in vitro* result, the *in vivo* RIG-I-IRF3/P-IRF3 signaling axis was determined by analyzing the protein level in the extracted tumors. Similar enhanced expression of RIG-I and P-IRF3/IRF3 ratio in the groups treated with PNRs or complex of PNRs and Poly I:C was observed after treatment (Fig. 8). The results demonstrate that MA-PNRplex enabled effective activation of the signaling axis of RIG-I-IRF3/P-IRF3 in the cancer cells *in vitro* and *in vivo*.

4. Discussion

4.1. Cytosolic delivery of Poly I:C to cancer cells rather than immune cells induces robust immunostimulation via activating RIG-I pathway

Poly I:C triggers immune response by activating toll-like-receptor ligand 3 (TLR-3) in the endosomal compartments of target cells, such as APCs, macrophages, fibroblasts, keratinocytes, muscle cells and liver cells, and promotion in antigen-presentation^{36,46–49}. Poly I:C can also be recognized by RIG-I in the cytoplasm of DCs and induces immunostimulation *via* the production of interferons⁴⁵. However, previous reports indicated that association of Poly I:C with RIG-I in non-immune cells induced modest immunostimulation^{18,39}. Unlike TLR-3 which locates in the endosomal compartment⁵⁰, RIG-I is a cytosolic pattern recognition receptor residing in the cytoplasm and has limited access to the ligand, Poly I:C⁵¹. Moreover, Poly I:C has poor stability and undergoes rapid enzymatic degradation in the endolysosomes, leading to little escape from the endosomes to the cytoplasm³⁶. In the study, *via* bypassing the endosomes, the PTX nanorods delivered Poly I:C to the cytoplasm with high efficacy and facilitated its association with the cytosolic RIG-I that subsequently activated the RIG-I-IRF3/P-IRF3 signaling axis. These results imply that only the ligands of RIG-I are delivered effectively to the cytosol, can the RIG-I signaling axis be activated to induce potent immunostimulation. In addition, cytosolic delivery of Poly I:C *via* endosomal escape mainly led to an induction of secretion of type I IFN, CXCL-10 and IL-10^{18,52}. In contrast, as depicted in Figs. 5 and 6, the administration of MA-PNRplex induced pronounced secretion of CCL-5, a proinflammatory chemokine that can recruit a variety of leukocytes into inflammatory sites and induce the activation and proliferation of particular natural killer cells⁵³. In contrast with the endosomal TLR-3, if the

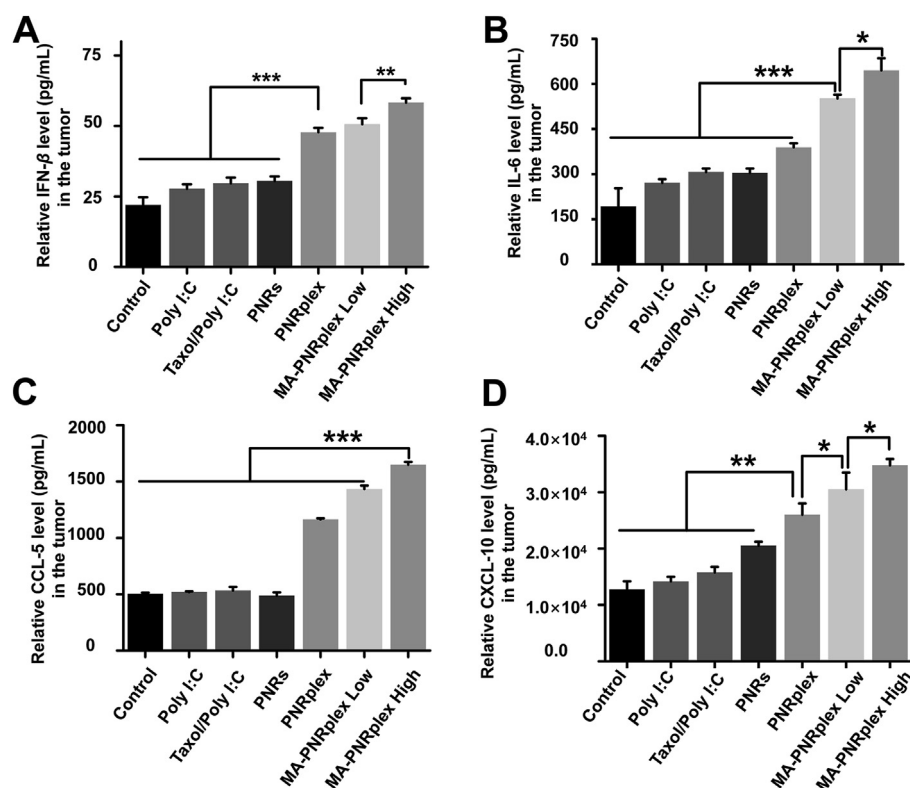


Figure 5 Cytokines and chemokines in the tumor. The tumors were collected at the end of treatment. The expression levels of these indicators were measured with ELISA Kit (mean \pm SEM, $n = 3$, * $P < 0.05$, ** $P < 0.01$ and *** $P < 0.001$).

cytosolic RIG-I pathway is activated potently, it may be more efficient to induce immunostimulation. The findings open a new path to promote immune response through activation of RIG-I-pathway in cancer cells.

4.2. Intracellularly sustaining release of cytotoxic agent significantly promotes immunogenicity of cancer cells

Conventional chemotherapy can impact the immune response via various mechanisms, including improving the immunogenicity of cancer cells, destroying immunosuppressive networks, and sensitizing cancer cells to immune cytotoxicity^{54,55}. Moreover, it was argued that long-term success of chemotherapy may rely on its induced immunostimulation⁵⁶. However, in the clinical practices, the paradox is that a high dose of administration is always required to kill cancer cells, and whereas, would lead to immunosuppressive side-effects. An administration strategy that can balance the two aspects is highly desirable. In this study, the administration of cytotoxic drug crystals, PNRs, not only effectively induced apoptosis of cancer cells, but also stimulated a strong immune response *via* promoted activation and recruitment of immune cells, including DCs, T-helper cells (CD4⁺), and cytotoxic T cells (CD8⁺), and enhanced secretion of immunomodulatory factors *in vitro* and *in vivo*. Unlike conventional drug carriers that release their cargoes rapidly after cellular uptake^{9,57}, the present drug crystals, PNRs, entered cells *via* bypassing the endosomes and continuously released the cytotoxic drug, PTX, overtime after internalization^{12,13,15}. The sustained-release profile in cells may reduce the toxicity of drug crystals to cancer cells,

extend the duration of immunogenic apoptosis and, as a result, facilitate the secretion of immunomodulatory factors, prolong their exposure to immune cells around and assist in attracting effector T cells into the tumor. Previous reports also demonstrated that *via* decreasing the toxicity of PTX by conjugating the drug with peptide or administration at a low dose⁵⁸, the immune response *in vitro* and *in vivo* was activated against cancer cells⁵⁹. Accordingly, we believe that the nanosized crystals of chemotherapy-induced immunotherapy. Furthermore, because of the facile preparation and scalability⁶⁰, the crystalized strategy has promising potential for clinical use.

4.3. Complex of cytotoxic pure drug nanocrystals/immunostimulant is a promising platform for chemoimmunotherapy due to asynchronous release after internalization

Increasing evidence showed chemoimmunotherapy has the potential to emerge as a renovated strategy to combat cancer. Frequently, chemoimmunotherapy can be achieved by two combinatorial regimens in which immunotherapy is used to neutralize the immunosuppressive effects or maximize the immunostimulatory potency of chemotherapy⁵⁶. However, such combinatorial approaches have little practical use in the clinic so far, although a combination of carboplatin or cisplatin, pemetrexed/pembrolizumab was approved for the treatment of non-small cancer cell cancer⁶¹. Co-delivery of chemotherapeutic agents and immunostimulants to cancer cells is one of the most convenient and universal strategies for chemoimmunotherapy due

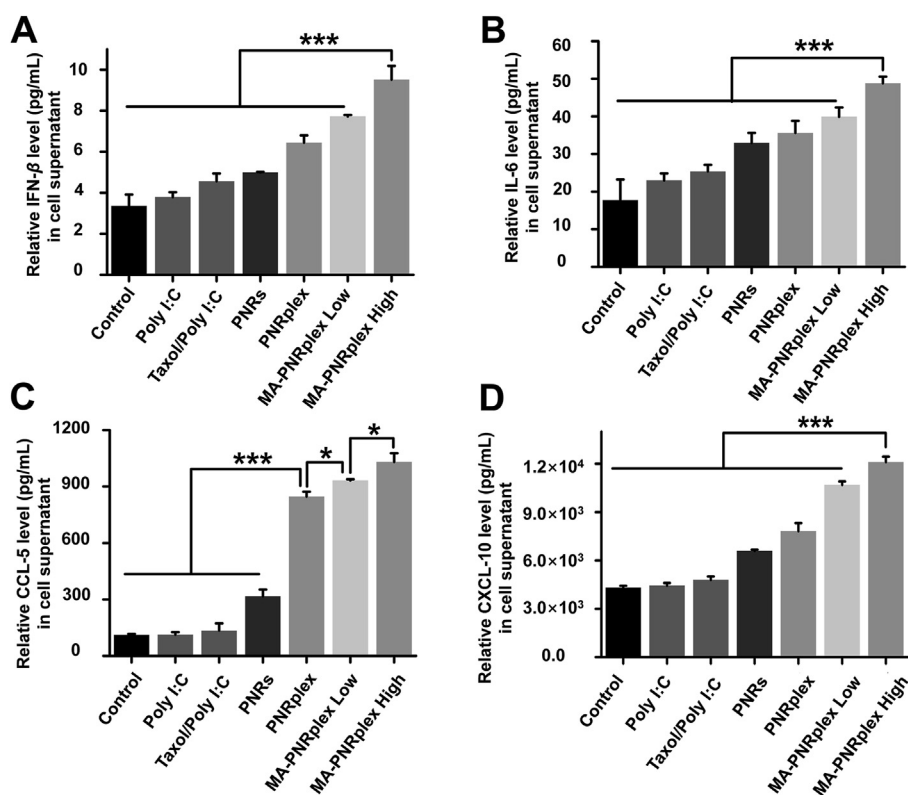


Figure 6 Immunostimulatory activity *in vitro*. Secretion *in vitro* of cytokines and chemokines determined by ELISA assay from B16F10 cells post-incubation with different formulations at a fixed PTX concentration of 10 $\mu\text{g}/\text{mL}$ and Poly I:C 2.5 $\mu\text{g}/\text{mL}$ at 37 $^{\circ}\text{C}$ for 12 h (mean \pm SEM, $n = 3$, $*P < 0.05$ and $***P < 0.001$). IFN- β (A), IL-6 (B), CCL-5 (C), and CXCL-10 (D).

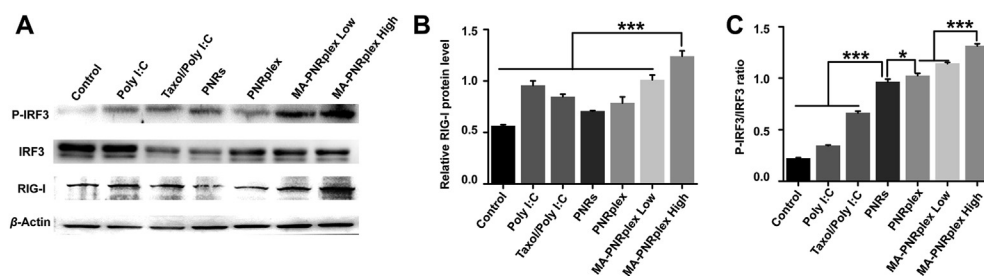


Figure 7 Activation of signaling pathway *in vitro*. Poly I:C-mediated expression *in vitro* of RIG-I, P-IRF-3 and IRF-3 examined by (A) WB analysis. Densitometric quantification of (B) RIG-I and (C) P-IRF-3/IRF-3 (mean \pm SEM, $n = 3$, $*P < 0.05$ and $***P < 0.001$). Protein levels were normalized to β -actin. The cells were treated with different formulations at a fixed PTX concentration of 10 $\mu\text{g}/\text{mL}$ and Poly I:C 2.5 $\mu\text{g}/\text{mL}$ at 37 $^{\circ}\text{C}$ for 12 h. The control group was treated with PBS.

to improved treatment outcomes and easy preparation. Noteworthy, the two active ingredients always have a spatiotemporal discrepancy in the cytosolic target and the exertion of activity. As a result, to maximize the synergy, asynchronous release of the two active agents from drug carriers is essential. Nonetheless, the currently used drug carriers inevitably release the two ingredients into the cytoplasm synchronously after uptake, compromising the synergistic effect^{62–65}. Our results in Fig. 1H and I and our previous reports^{13,15} implicated that the complex of drug nanocrystals/biologics characterized the asynchronous release of the two active agents, where the drug release from the drug crystals lasted >70 h whereas the release of biological drug was

completed within 2 h. After internalization, the drug crystals continuously released the drug for 7–10 h^{11,12}; in contrast with the *in vitro* release, the release period in cells was markedly shortened, probably induced by the interplay with the endogenous substance. The intracellular release of the two active drugs from the complex was asynchronous. No co-delivery systems are reported to have this property so far. As our best knowledge, adjusting the ratio between PTX and Poly I:C in drug carriers is the only feasible strategy to improve the synergy. However, the conventional carriers have extremely low drug-loading capacity at less than 10% which significantly weakened this ability. The present study provided a potent approach to enhance the synergy

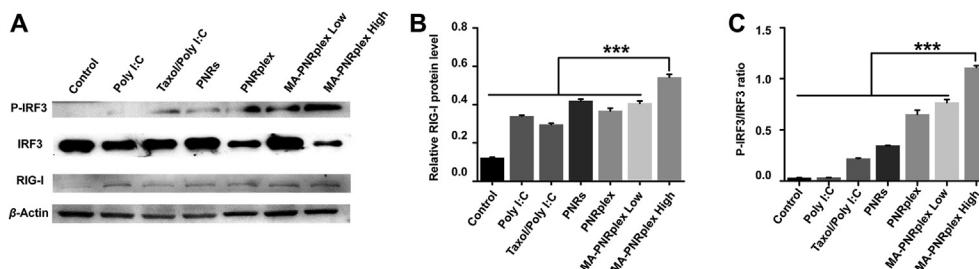


Figure 8 Activation of signaling pathway *in vivo*. Expression *in vivo* of RIG-I, P-IRF-3 and IRF-3 in the tumor determined by (A) WB assay. Quantitative analysis of (B) RIG-I and (C) P-IRF-3/IRF-3 (mean \pm SEM, $n = 3$, $***P < 0.001$). Protein levels were normalized to β -actin. The tumors were collected from mice at the end of the treatment. The control group was treated with saline.

of two drugs. In addition, accumulating evidence implied that biological drugs often take much longer time to exert their activities after uptake compared with small molecular drugs⁶⁶. Therefore, the platform is promising to maximize the synergy between chemotherapy and immunotherapy. In our study, the synergy was indeed confirmed in the cytotoxicity as displayed by the combination index (CI, Supporting Information Fig. S8).

5. Conclusions

In this study, we demonstrated that cytosolic delivery of Poly I:C with drug nanocrystals to cancer cells rather than immune cells significantly activated the RIG-I signaling axis and induced profound immunostimulation. The findings unveil that increasing the accessibility of cytosolic RIG-I in cancer cells to its ligands allows for improved immune response. Intracellular sustained-release of cytotoxic agent from its pure crystals in cancer cells enables strong immunostimulatory potency. The crystallization of cytotoxic agent represents a promising approach to facilitate the clinic practice of chemotherapy-induced immunotherapy *via* avoiding durable low-dose metronomic administration. Furthermore, cytosolic delivery of the complex of cytotoxic drug nanocrystals/immunostimulant confers the asynchronous release of the two active agents and markedly amplifies the immune response. The developed asynchronous-release co-delivery system with extremely high drug-loading capacity has potential to overcome the disadvantages of currently used regimen of chemoimmunotherapy that frequently requires subsequent administration of chemotherapeutic agent and immunostimulant and long-lasting administration of the cytotoxic drug. Taken together, the present co-delivery system offers a novel strategy to potentially maximize chemoimmunotherapy.

Acknowledgments

This study was supported by the National Natural Science Foundation of China (Nos. 81872823, 81871477 and 82073782), the Double First-Class (CPU2018PZQ13, China) of the CPU, the Shanghai Science and Technology Committee (19430741500, China), and the Key Laboratory of Modern Chinese Medicine Preparation of Ministry of Education of Jiangxi University of Traditional Chinese Medicine (TCM-201905, China).

Author contributions

Wei He conceived and designed the work. Xiaoqing Du, Yuqi Hou, Jia Huang, Yan Pang, and Chenlu Ruan performed the

experiments. Wei He and Xiaoqing Du co-wrote the paper. Wei Wu, Chenjie Xu, Hongwei Zhang, and Lifang Yin commented and corrected the paper. All of the authors have read and approved the final manuscript.

Conflicts of interest

The authors have no conflicts of interest to declare.

Appendix A. Supporting information

Supporting data to this article can be found online at <https://doi.org/10.1016/j.apsb.2021.03.014>.

References

1. He W, Kapate N, IV CWS, Mitragotri S. Drug delivery to macrophages: a review of targeting drugs and drug carriers to macrophages for inflammatory diseases. *Adv Drug Deliv Rev* 2020;**165**:15–40.
2. Xiao Q, Li X, Li Y, Wu Z, Xu C, Chen Z, et al. Biological drug and drug delivery-mediated immunotherapy. *Acta Pharm Sin B* 2021;**11**:941–60.
3. Zhu Y, Yu X, Thamphiwatana SD, Zheng Y, Pang Z. Nanomedicines modulating tumor immunosuppressive cells to enhance cancer immunotherapy. *Acta Pharm Sin B* 2020;**10**:2054–74.
4. Duan X, Chan C, Lin W. Nanoparticle-mediated immunogenic cell death enables and potentiates cancer immunotherapy. *Angew Chem Int Ed* 2019;**58**:670–80.
5. Riley RS, June CH, Langer R, Mitchell MJ. Delivery technologies for cancer immunotherapy. *Nat Rev Drug Discov* 2019;**18**:175–96.
6. Qi J, Hu X, Dong X, Lu Y, Lu H, Zhao W, et al. Towards more accurate bioimaging of drug nanocarriers: turning aggregation-caused quenching into a useful tool. *Adv Drug Deliv Rev* 2019;**143**:206–25.
7. Xiao Q, Zhu X, Yuan Y, Yin L, He W. A drug-delivering-drug strategy for combined treatment of metastatic breast cancer. *Nanomed-Nanotechnol* 2018;**14**:2678–88.
8. Donahue ND, Acar H, Wilhelm S. Concepts of nanoparticle cellular uptake, intracellular trafficking, and kinetics in nanomedicine. *Adv Drug Deliv Rev* 2019;**143**:68–96.
9. He W, Xing X, Wang X, Wu D, Wu W, Guo J, et al. Nanocarrier-mediated cytosolic delivery of biopharmaceuticals. *Adv Funct Mater* 2020;**30**:201910566.
10. Zhao Z, Ukidve A, Krishnan V, Mitragotri S. Effect of physicochemical and surface properties on *in vivo* fate of drug nanocarriers. *Adv Drug Deliv Rev* 2019;**143**:3–21.
11. Teng C, Lin C, Huang F, Xing X, Chen S, Ye L, et al. Intracellular codelivery of anti-inflammatory drug and anti-miR 155 to treat inflammatory disease. *Acta Pharm Sin B* 2020;**10**:1521–33.
12. Xin X, Du X, Xiao Q, Azevedo HS, He W, Yin L. Drug nanorod-mediated intracellular delivery of microRNA-101 for self-sensitization *via* autophagy inhibition. *Nano-Micro Lett* 2019;**11**:82.

13. Xin X, Pei X, Yang X, Lv Y, Zhang L, He W, et al. Rod-shaped active drug particles enable efficient and safe gene delivery. *Adv Sci* 2017;**4**: 1700324.
14. Mohammad IS, Teng C, Chaurasiya B, Yin L, Wu C, He W. Drug-delivering-drug approach-based codelivery of paclitaxel and disulfiram for treating multidrug-resistant cancer. *Int J Pharm* 2019;**557**: 304–13.
15. Xin X, Teng C, Du X, Lv Y, Xiao Q, Wu Y, et al. Drug-delivering-drug platform-mediated potent protein therapeutics via a non-endolysosomal route. *Theranostics* 2018;**8**:3474–89.
16. Pfannenstiel LW, Lam SSK, Emens LA, Jaffee EM, Armstrong TD. Paclitaxel enhances early dendritic cell maturation and function through TLR4 signaling in mice. *Cell Immunol* 2010;**263**:79–87.
17. Wang TH, Chan YH, Chen CW, Kung WH, Lee YS, Wang ST, et al. Paclitaxel (Taxol) upregulates expression of functional interleukin-6 in human ovarian cancer cells through multiple signaling pathways. *Oncogene* 2006;**25**:4857–66.
18. Glas M, Coch C, Trageser D, DaBler J, Simon M, Koch P, et al. Targeting the cytosolic innate immune receptors RIG-I and MDA5 effectively counteracts cancer cell heterogeneity in glioblastoma. *Stem Cell* 2013;**31**:1064–74.
19. Zhang Y, Li N, Chen Q, Yan K, Liu Z, Zhang X, et al. Breakdown of immune homeostasis in the testis of mice lacking Tyro 3, Axl and Mer receptor tyrosine kinases. *Immunol Cell Biol* 2013;**91**:416–26.
20. Guo Z, Chen L, Zhu Y, Zhang Y, He S, Qin J, et al. Double-stranded RNA-induced TLR3 activation inhibits angiogenesis and triggers apoptosis of human hepatocellular carcinoma cells. *Oncol Rep* 2012;**27**:396–402.
21. Palladino M, Johnson T, Gupta R, Chapman J, Ojha P. Members of the Toll-like receptor family of innate immunity pattern-recognition receptors are abundant in the male rat reproductive tract. *Biol Reprod* 2007;**76**:958–64.
22. Zhu W, Chen Q, Yan K, Liu Z, Li N, Zhang X, et al. RIG-I-like receptors mediate innate antiviral response in mouse testis. *Mol Endocrinol* 2013;**27**:1455–67.
23. He W, Lu Y, Qi J, Chen L, Hu F, Wu W. Food proteins as novel nanosuspension stabilizers for poorly water-soluble drugs. *Int J Pharm* 2013;**441**:269–78.
24. He W, Tan Y, Tian Z, Chen L, Hu F, Wu W. Food protein-stabilized nanoemulsions as potential delivery systems for poorly water-soluble drugs: preparation, *in vitro* characterization, and pharmacokinetics in rats. *Int J Nanomed* 2011;**6**:521–33.
25. Lv Y, Xu C, Zhao X, Lin C, Yang X, Xin X, et al. Nanoplatform assembled from a CD44-targeted prodrug and smart liposomes for dual targeting of tumor microenvironment and cancer cells. *ACS Nano* 2018;**12**:1519–36.
26. Roy A, Chandra S, Mamilapally S, Upadhyay P, Bhaskar S. Anti-cancer and immunostimulatory activity by conjugate of paclitaxel and non-toxic derivative of LPS for combined chemo-immunotherapy. *Pharm Res (N Y)* 2012;**29**:2294–309.
27. Ye J, Dong W, Yang Y, Hao H, Liao H, Wang B, et al. Vitamin E-rich nanoemulsion enhances the antitumor efficacy of low-dose paclitaxel by driving Th1 immune response. *Pharm Res (N Y)* 2017;**34**:1244–54.
28. Zhang L, Yang X, Lv Y, Xin X, Qin C, Han X, et al. Cytosolic codelivery of miRNA-34a and docetaxel with core-shell nanocarriers via caveolae-mediated pathway for the treatment of metastatic breast cancer. *Sci Rep* 2017;**7**:46186.
29. Parton RG, Richards AA. Lipid rafts and caveolae as portals for endocytosis: new insights and common mechanisms. *Traffic* 2003;**4**: 724–38.
30. Cheng YS, Xu F. Anticancer function of polyinosinic-polycytidylic acid. *Cancer Biol Ther* 2010;**10**:1219–23.
31. Verdijk RM, Mutis T, Esendam B, Kamp J, Melief CJM, Brand A, et al. Polyriboinosinic polyribocytidylic acid (poly(I:C)) induces stable maturation of functionally active human dendritic cells. *J Immunol* 1999;**163**:57–61.
32. Takagi S, Takahashi Y, Sugimura K, Nishikawa M, Takakura Y. Application of magnesium pyrophosphate-based sponge-like micro-particles to enhance the delivery efficiency and adjuvant effects of polyriboinosinic-polyribocytidylic acid in immune cells. *J Pharmacol Sci* 2016;**105**:766–72.
33. Zhu ZY, Jia CZ, Luo JM, Wang L. Polyriboinosinic-polyribocytidylic acid facilitates interleukin-6, and interleukin-8 secretion in human dermal fibroblasts via the JAK/STAT3 and p38 MAPK signal transduction pathways. *Cytokine* 2018;**102**:1–6.
34. Peine KJ, Bachelder EM, Vangundy Z, Papenfuss T, Brackman DJ, Gallovic MD, et al. Efficient delivery of the toll-like receptor agonists polyinosinic: polycytidylic acid and CpG to macrophages by aceta-lated dextran microparticles. *Mol Pharm* 2013;**10**:2849–57.
35. Steinhagen F, Kinjo T, Bode C, Klinman DM. TLR-based immune adjuvants. *Vaccine* 2011;**29**:3341–55.
36. Hafner AM, Corthésy B, Merkle HP. Particulate formulations for the delivery of poly (I:C) as vaccine adjuvant. *Adv Drug Deliv Rev* 2013;**65**:1386–99.
37. Ammi R, De Waele J, Willems Y, Van Brussel I, Schrijvers DM, Lion E, et al. Poly (I:C) as cancer vaccine adjuvant: knocking on the door of medical breakthroughs. *Pharmacol Ther* 2015;**146**:120–31.
38. Lewis SM, Williams A, Eisenbarth SC. Structure and function of the immune system in the spleen. *Sci Immunol* 2019;**4**:eaau6085.
39. Duwell P, Steger A, Lohr H, Bourhis H, Hoelz H, Kirchleitner SV, et al. RIG-I-like helicases induce immunogenic cell death of pancreatic cancer cells and sensitize tumors toward killing by CD8⁺ T cells. *Cell Death Differ* 2014;**21**:1825–37.
40. Dmitrieva O, Shilovskiy I, Khaitov M, Grivennikov S. Interleukins 1 and 6 as main mediators of inflammation and cancer. *Biochemistry (Mosc)* 2016;**81**:80–90.
41. Tanaka T, Narazaki M, Kishimoto T. IL-6 in inflammation, immunity, and disease. *Cold Spring Harbor Perspect Biol* 2014;**6**:a016295.
42. Lunardi S, Lim SY, Muschel RJ, Brunner TB. IP-10/CXCL10 attracts regulatory T cells: implication for pancreatic cancer. *Oncol Immunology* 2015;**4**:e1027473.
43. Balkwill F. Cancer and the chemokine network. *Nat Rev Cancer* 2004;**4**:540–50.
44. Okahira S, Nishikawa F, Nishikawa S, Akazawa T, Seya T, Matsumoto M. Interferon- β induction through Toll-like receptor 3 depends on double-stranded RNA structure. *DNA Cell Biol* 2005;**24**:614–23.
45. Kato H, Takeuchi O, Sato S, Yoneyama M, Yamamoto M, Matsui K, et al. Differential roles of MDA5 and RIG-I helicases in the recognition of RNA viruses. *Nature* 2006;**441**:101–5.
46. Blander JM, Medzhitov R. Toll-dependent selection of microbial antigens for presentation by dendritic cells. *Nature* 2006;**440**:808–12.
47. Sokolova V, Shi Z, Huang S, Du Y, Kopp M, Frede A, et al. Delivery of the TLR ligand poly(I:C) to liver cells *in vitro* and *in vivo* by calcium phosphate nanoparticles leads to a pronounced immunostimulation. *Acta Biomater* 2017;**64**:401–10.
48. Luo Z, Wang C, Yi H, Li P, Pan H, Liu L, et al. Nanovaccine loaded with poly I:C and STAT3 siRNA robustly elicits anti-tumor immune responses through modulating tumor-associated dendritic cells *in vivo*. *Biomaterials* 2015;**38**:50–60.
49. Speth MT, Repnik U, Griffiths G. Layer-by-layer nanocoating of live Bacille-Calmette-Guérin mycobacteria with poly(I:C) and chitosan enhances pro-inflammatory activation and bactericidal capacity in murine macrophages. *Biomaterials* 2016;**111**:1–12.
50. Zhou Z, Lin H, Li C, Wu Z. Recent progress of fully synthetic carbohydrate-based vaccine using TLR agonist as build-in adjuvant. *Chin Chem Lett* 2018;**29**:19–26.
51. Heidegger S, Wintges A, Stritzke F, Bek S, Steiger K, Koenig PA, et al. RIG-I activation is critical for responsiveness to checkpoint blockade. *Sci Immunol* 2019;**4**:eaau8943.
52. Chattopadhyay S, Liu YH, Fang ZS, Lin CL, Lin JC, Yao BY, et al. Synthetic immunogenic cell death mediated by intracellular delivery of STING agonist nanoshells enhances anticancer chemo-immunotherapy. *Nano Lett* 2020;**20**:2246–56.

53. Soria G, Ben-Baruch A. The inflammatory chemokines CCL2 and CCL5 in breast cancer. *Cancer Lett* 2008;**267**:271–85.
54. Luo Q, Zhang L, Luo C, Jiang M. Emerging strategies in cancer therapy combining chemotherapy with immunotherapy. *Cancer Lett* 2019;**454**:191–203.
55. Li J, Burgess DJ. Nanomedicine-based drug delivery towards tumor biological and immunological microenvironment. *Acta Pharm Sin B* 2020;**11**:2110–24.
56. Galluzzi L, Buque A, Kepp O, Zitvogel L, Kroemer G. Immunological effects of conventional chemotherapy and targeted anticancer agents. *Cancer Cell* 2015;**28**:690–714.
57. Zhuang J, Wang D, Li D, Yang Y, Lu Y, Wu W, et al. The influence of nanoparticle shape on bilateral exocytosis from Caco-2 cells. *Chin Chem Lett* 2018;**29**:1815–8.
58. Zhong H, Han B, Tourkova IL, Lokshin A, Rosenbloom A, Shurin MR, et al. Low-dose paclitaxel prior to intratumoral dendritic cell vaccine modulates intratumoral cytokine network and lung cancer growth. *Clin Cancer Res* 2007;**13**:5455–62.
59. Tang W, Yang J, Yuan Y, Zhao Z, Lian Z, Liang G. Paclitaxel nanoparticle awakens immune system to fight against cancer. *Nanoscale* 2017;**9**:6529–36.
60. Lu Y, Lv Y, Li T. Hybrid drug nanocrystals. *Adv Drug Deliv Rev* 2019; **143**:115–33.
61. Reck M, Bondarenko I, Luft A, Serwatowski P, Barlesi F, Chacko R, et al. Ipilimumab in combination with paclitaxel and carboplatin as first-line therapy in extensive-disease-small-cell lung cancer: results from a randomized, double-blind, multicenter phase 2 trial. *Ann Oncol* 2013;**24**:75–83.
62. Yin Y, Hu Q, Xu C, Qiao Q, Qin X, Song Q, et al. Co-delivery of doxorubicin and interferon- γ by thermosensitive nanoparticles for cancer immunochemotherapy. *Mol Pharm* 2018;**15**:4161–72.
63. Zhang D, Wu T, Qin X, Qiao Q, Shang L, Song Q, et al. Intracellularly generated immunological gold nanoparticles for combinatorial photothermal therapy and immunotherapy against tumor. *Nano Lett* 2019; **19**:6635–46.
64. Yang X, Hu C, Tong F, Liu R, Zhou Y, Qin L, et al. Tumor microenvironment-responsive dual drug dimer-loaded PEGylated bilirubin nanoparticles for improved drug delivery and enhanced immunotherapy of breast cancer. *Adv Funct Mater* 2019;**29**:1901896.
65. Yin J, Cao H, Wang H, Sun K, Li Y, Zhang Z. Phospholipid membrane-decorated deep-penetrated nanocatalase relieve tumor hypoxia to enhance chemo-photodynamic therapy. *Acta Pharm Sin B* 2020;**10**:2246–57.
66. He CL, Tang ZH, Tian HY, Chen XS. Co-delivery of chemotherapeutics and proteins for synergistic therapy. *Adv Drug Deliv Rev* 2016; **98**:64–76.